Supporting Information

Knitting-Stitching Bifacial Metafabric with Switchable Thermal and Moisture Transmissibility for Multimodal Dynamic Personal Thermoregulation

Benhui Li[1], Mengdi Wang[1], Shuyu Ao[1], Kuan Lyu[1], Xuzhong Su[1*], Fengxin Sun[1,2*]

1. Laboratory of Soft Fibrous Materials and Physics, College of Textile Science and Engineering, Jiangnan University, Wuxi 214122, China.
2. MOE Key Laboratory of Special Protection Textiles, Jiangnan University, Wuxi 214122, China.

Email: fxsun@jiangnan.edu.cn; mfgucv@163.com

Supplementary Note 1. Preparation of knitted fabrics.

Janus double-layer fabrics are knitted on computerized flat knitting machines. By choosing 150D PLA yarns and silver-plated nylon yarns as the raw materials, the two yarns are guided to the front and back needle beds through the yarn guides during the knitting process, and knitted on different sides of the fabric. The wettability and emissivity of each side depends on the properties of the yarns used on that side, giving the fabric its unique functionality. At the completion of each of the six loop forming cycles, the outer fabric is connected to the lower fabric by means of loop gathering, creating a tight and stable structure. In the final stage of the weaving process, the front and back needles are synchronized to ensure that the upper and lower fabric layers are knitted together, thus ensuring the integrity of the fabric. Upon completion of the knitting process, the yarn fed from the front needle bed is presented on the front side of the fabric, while the yarn from the back needle bed is presented on the back side of the fabric, as shown in Figure S1.

Supplementary Note 2. Calculation of optical properties of fabrics.

We use Kirchhoff's law to calculate the emissivity of textiles. Kirchhoff's law of thermal radiation describes the relationship between the emission ratio and the absorption ratio of an object, that is, the emission ratio of an object is equal to its absorption ratio for the same wavelength in a state of thermodynamic equilibrium. Based on this principle, we use the following formula to calculate the emissivity of textiles.

$$A_\lambda + R_\lambda + T_\lambda = 1 \tag{S1}$$

$$E_\lambda = A_\lambda \tag{S2}$$

where E_λ, A_λ, R_λ, and T_λ represent the emissivity, absorptivity, reflectivity, and transmittance of the sample, respectively. Considering that the transmittance of the fabrics is very low due to their relatively large thickness, we assume $T_\lambda = 0$, and thus the emissivity can be calculated by,

$$E\lambda = 1 - R\lambda \tag{S3}$$

Supplementary Note 3. Cooling power calculation method.

Theoretical cooling power is calculated by one-dimensional steady state energy balance model (Equation S4):

$$P_{cool}(T) = P_{rad}(T) - P_{atm}(T_{amb}) - P_{sun} - P_{non-rad} \tag{S4}$$

where P_{cool} is the theoretical cooling power, P_{rad} represents the power radiated from the radiant cooler at temperature T, P_{atm} is the absorbed atmospheric emitted power at the surface of the radiant cooler, P_{sun} is the absorbed solar irradiation, and P_{nonrad} is the non-radiative (conduction and convective) heat gain of the radiant cooler. P_{cool}, P_{atm}, P_{sun}, and $P_{non-rad}$ can be calculated by equations S4-S10:

$$P_{rad}(T) = 2\pi \int_0^{\frac{\pi}{2}} \mathrm{d}\theta \sin\theta \cos\theta \int_{2.5\mathrm{um}}^{25\mathrm{um}} I_{\mathrm{BB}}(\mathrm{T},\lambda)\varepsilon(\lambda,\theta)d\theta \tag{S5}$$

$$I_{BB}(T,\lambda) = \frac{2\mathrm{hc}^2}{\lambda^5} \frac{1}{\mathrm{e}^{hc/\lambda K_B T} - 1} \tag{S6}$$

$$P_{atm}(T_{amb}) = 2\pi \int_0^{\frac{\pi}{2}} d\theta \sin\theta \cos\theta \int_{2.5um}^{25um} I_{BB}(T,\lambda)\varepsilon_{atm}(\lambda,\theta)d\lambda \tag{S7}$$

$$\varepsilon_{atm}(\lambda,\theta) = 1 - t(\lambda)^{1/\cos\theta} \tag{S8}$$

$$P_{sun} = \int_{0.25um}^{2,5um} (1 - R(\lambda))E_{sol}(\lambda)d\lambda \tag{S9}$$

$$P_{non-rad} = hc(T_{amb} - T) \tag{S10}$$

Where P_{rad} (T) represents the power radiated out by the radiative cooler at temperature T, I_{BB} (T, λ) is the spectral radiance of a blackbody at temperature T, ε (λ, θ) is the spectral and angular emissivity of the cooler. h is Planck's constant, K_B is Boltzmann constant, and c is the speed of light. P_{atm} (T_{amb}) is the Atmospheric thermal radiation absorbed by the radiative cooler. where t (λ, 0) is the normal atmospheric transmittance that can be obtained by MODTRAN (atmospheric transmittance at RH = 20% is plotted in Figure S2), R (λ) is the solar reflectivity of radiative cooler, Esol (λ)

is the ASTM G173 global solar intensity spectrum, hc is the non-radiative heat transfer coefficient, T_{amb} is the ambient temperature.

Supporting Figures S1-S11

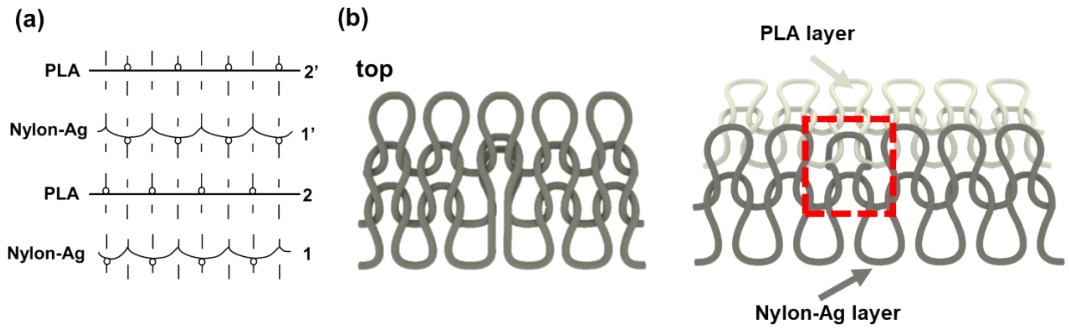

Figure S1. Structure illustration of bifacial knit fabric. (a) Janus bifacial fabric structure and knitting diagram. (b) Structural illustration of the knitted fabrics.

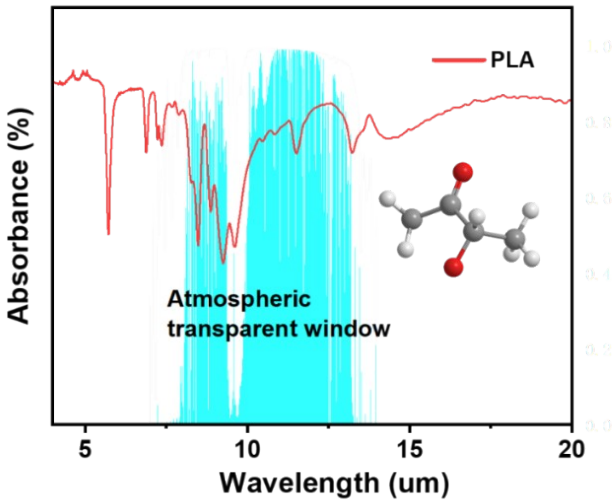

Figure S2. Structure of PLA and spectral absorption.

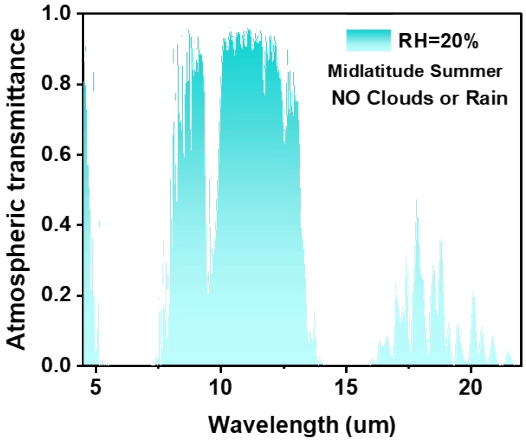

Figure S3. Atmospheric transmittance in the region of 2.5-25 μm. The date is obtained from MODTRAN when the relative humidity (RH) is 20%. The ambient temperature is set to 298 K.

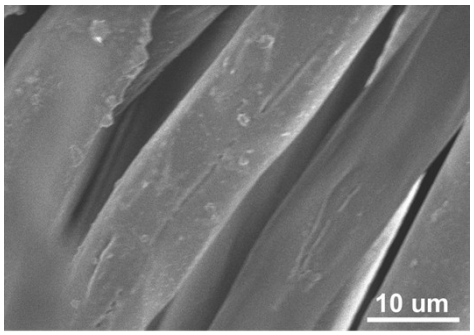

Figure S4. SEM image of PLA fiber surface.

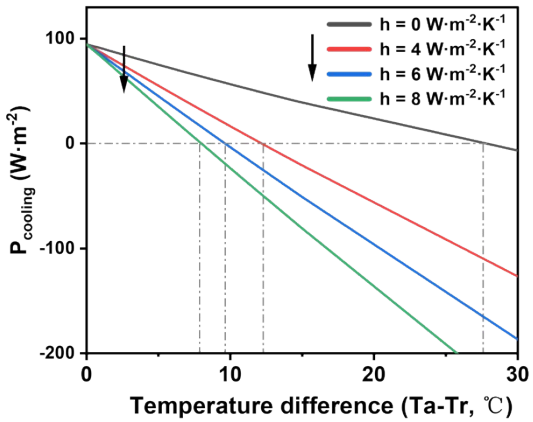

Figure S5. Theoretical cooling capacity of TMM fabrics indicated by relationship between the cooling power (Pcooling) and temperature difference between the fabric

(Ta) and ambience (Tr) under different heat transfer coefficients (ambient temperature set at 300 K).

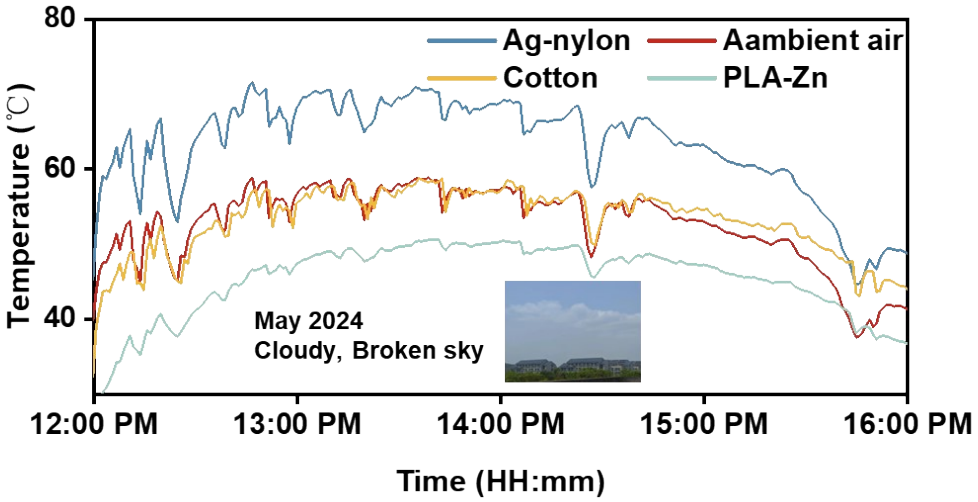

Figure S6. Outdoor thermal measurements of TMM fabrics on a cloudy day (April, Wuxi, China).

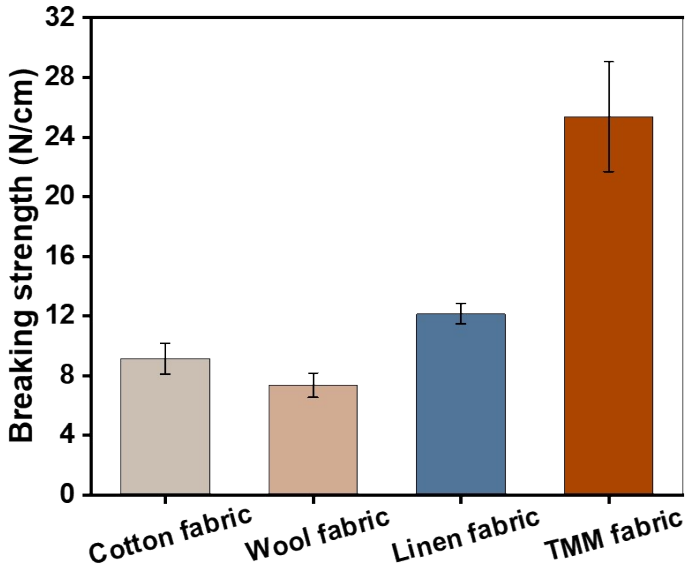

Figure S7. Comparison of strength between the TMM fabric with certain commercial fabrics, such as cotton fabric, wool fabric and linen fabric.

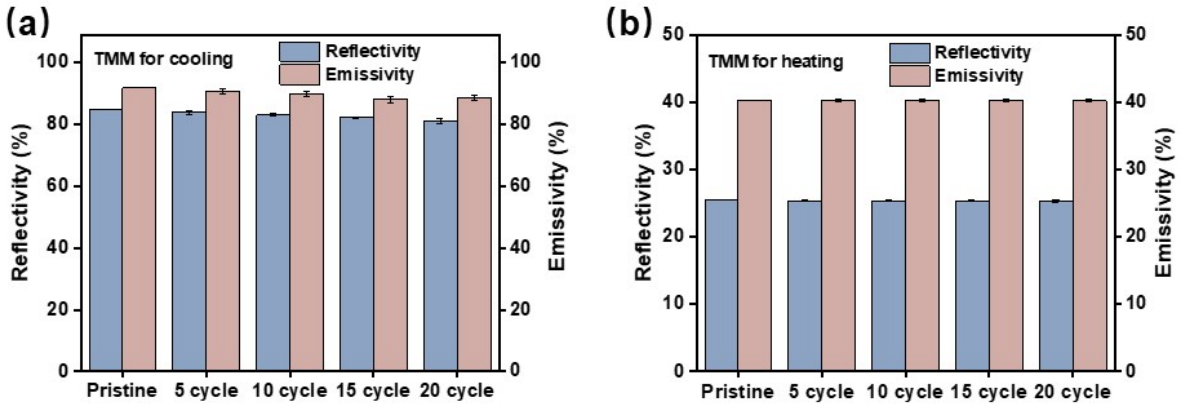

Figure S8. Washing durability. (a) Solar reflectance and mid-infrared emissivity of the cooling side of TMM fabrics against 20-cycle washes. (b) Solar reflectivity and mid-infrared emissivity of the heating side of TMM fabrics against 20-cycle washes. After several washes, the optical properties of the TMM fabrics showed only minor changes compared to its initial state.

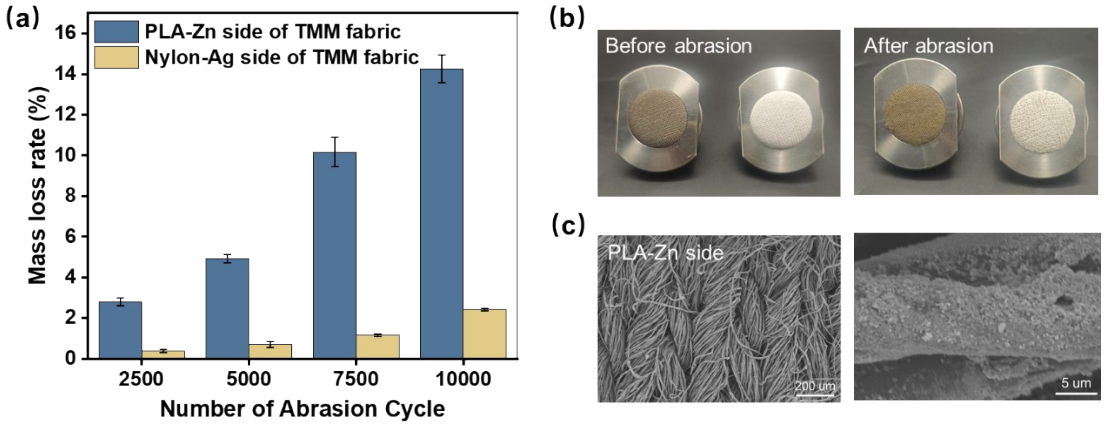

Figure S9. Wear resistance test of TMM fabrics. (a) Mass loss rate of the fabric after certain numbers of wearing cycles on different sides of the TMM fabrics. (b) Comparison of optical images of the TMM fabrics before and after abrasion testing. (c) SEM image of PLA-Zn side after abrasion test. The reasonably low mass loss rates (around 0.4% to 2.4% for the nylon-Ag side and 2.8% to 14.2% for the PLA-Zn side, respectively, after 2500 to 10000 abrasion cycles) indicate the desirable wear resistance of the TMM fabrics.

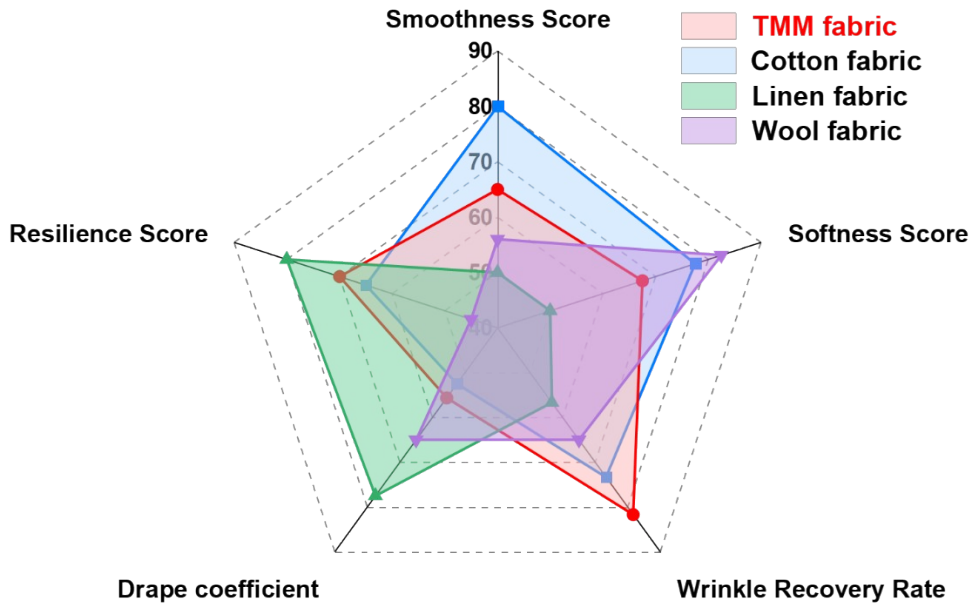

Figure S10. Comparison of the fabric handle values between the TMM fabric with certain commercial fabrics based on PhabrOmeter testing. The larger ranking value, the better resilience, softness and smoothness handle for the sample will be. The TMM fabric shows comparable resilience, softness, and smoothness handle characteristics to natural fiber-based fabrics.

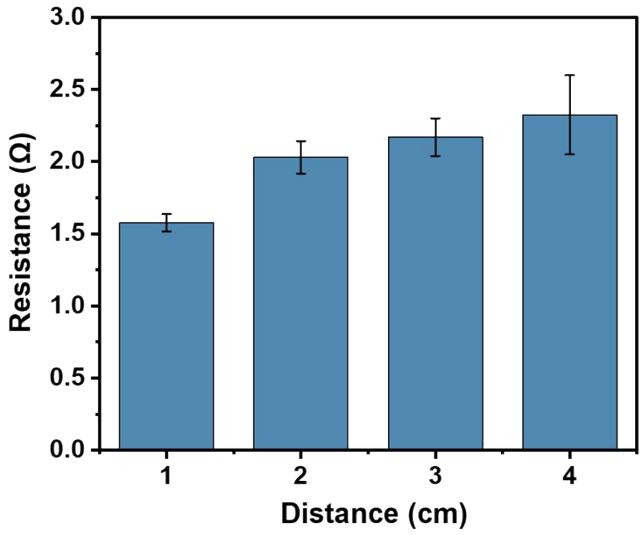

Figure S11. Resistance (Ω) versus distance of the Nylon-Ag surface of the TMM fabric.

Supporting Tables S1-S2

Table S1 Estimated material cost of the TMM fabrics

Materials	Price （$ /kg）	Dosage（kg/m^2）	Cost（$/m^2）
Polylactic acid yarn	3.2~8.5/kg	0.11 kg	0.3~0.9
Nylon-Ag yarn	50~122/kg	0.10 kg	5.0~12.2
ZnO nanoparticles	12.1~31.4/kg	0.05 kg	0.6~1.6
	Total		5.9~14.7

Note: According to the prices listed on www.alibaba.com, accessed in October 2024

Table S2. Comparison of the TMM fabric with recently reported passive warming/cooling materials

Materials/ Structures	Radiative cooling /warming	Evaporative cooling	Processing methods	Cost [#]	Ref.
PU-Si_3N_4-CM / Multi-layer thin film	√/×	√	Electrospinning (slow)	High	S1
PLA/Aerogel	√/×	×	Phase separation	Moderate	S2
CS-SiO_2/Woven	√/×	×	Wet spinning	Moderate	S3
Au-Ge-nPE/Thin film	×/√	×	Vacuum deposition	Very high	S4
SEBS-Al_2O_3/ Nonwoven	√/×	√	Electrospinning/ Lamination	Moderate	S5
PLA-CA-MSi_3N_4/Thin film	√/×	√	Electrospinning	High	S6
Ag-CNT-ZnO-PVDF/Thin film	√/√	×	Electrospinning/Spray coating	High	S7
PLA-TiO_2-AgNWs	√/√	√	Electrospinning/Hydrothermal reduction	High	S8
PLA-ZnO-Nylon-Ag/Knit	√/√	√	**Knitting/Spray coating**	**Low**	**This work**

[#]**Note:** The cost assertions in Table S2 are explained below.

Cost:

The cost involves two parts, namely, materials and manufacturing costs. Fabrication of radiative cooling materials relies on two types of key substrates. One is polymeric materials that exhibit high emissive properties in the wavelength range of the atmospheric transparency window (8-13 um), including PU (Ref. S1), Chitosan (Ref. S2), PVDF (Ref. S7), and PLA (Refs. S2, S6, and S8). PLA yarns are reasonably priced, ranging from $3.28/kg to $8.5/kg, (according to the prices listed on www.alibaba.com, accessed in October 2024). The other is metal oxides and nanoparticles, which are used to reflect solar radiation, including ZnO ($12.1/kg to $31.4/kg), Al_2O_3 ($20/kg to $37/kg), and TiO_2 ($17.1/kg to 30.7/kg). In addition, radiative warming technology relies on key materials that are characterized by their ability to reflect heat radiated from the body. Previous research has intensively used materials such as silver nanowire, graphene and Mxene. In comparison, the silver-plated conductive yarns (≈ $50/kg) used in our study is relatively cost-effective.

Regarding manufacturing cost, the commonly used methods for manufacturing radiative cooling and warming materials include electrostatic spinning (Ref. S1, S5, S6, S7, S8), vacuum deposition (Ref. S4), and wet-spinning (Ref. S3). These methods generally suffer from complex and time-consuming processing, low scalability, and thus lead to high cost, which makes it difficult to meet the demands and efficiency standards of large-scale industrialized production. In contrast, TMM fabrics utilize industrial knitting technology by integrating yarns with different optical properties into our designed structure, which significantly reduce the manufacturing cost of the TMM fabrics. Moreover, the high scalability of the textile manufacturing process also contributes to the low cost.

Supporting References

S1. D. Miao, N. Cheng, X. Wang, J. Yu and B. Ding, *Nano Lett.*, 2022, **22**, 680-687.

S2. X. Liu, M. Zhang, Y. Hou, Y. Pan, C. Liu and C. Shen, *Advanced Functional Materials*, 2022, **32**, 2207414.

S3. C. Chen, X. Jia, X. Li, M. Shi, J. Hu, M. Song, S. Wu, H. Dai, X. Wang and H. Geng, *Chem. Eng. J.*, 2023, **475**, 146307.

S4. H. Luo, Q. Li, K. Du, Z. Xu, H. Zhu, D. Liu, L. Cai, P. Ghosh and M. Qiu, *Nano Energy*, 2019, **65**, 103998.

S5. C. Fan, Y. Zhang, Z. Long, A. Mensah, Q. Wang, P. Lv and Q. Wei, *Advanced Functional Materials*, 2023, **33**, 2300794.

S6. P. Yang, Y. Ju, J. He, Z. Xia, L. Chen and S. Tang, *Advanced Fiber Materials*, 2024, 1-12.

S7. Y.-N. Song, M.-Q. Lei, D.-L. Han, Y.-C. Huang, S.-P. Wang, J.-Y. Shi, Y. Li, L. Xu, J. Lei and Z.-M. Li, *ACS Appl. Mater. Interfaces*, 2021, **13**, 19301-19311.

S8. S. Feng, L. Yao, X. Chen, C. Liu, X. Bu, Y. Huang, M. He and Y. Zhou, *J. Colloid Interface Sci.*, 2023, **648**, 117-128.